ACS APPLIED MATERIALS & INTERFACES

www.acsami.org

Research Article

One-Pot Synthesis of CHA/ERI-Type Zeolite Intergrowth from a Single Multiselective Organic Structure-Directing Agent

Soonhyoung Kwon, Estefanía Bello-Jurado, Evgeniia Ikonnikova, Hwajun Lee, Daniel Schwalbe-Koda, Avelino Corma, Tom Willhammar, Elsa A. Olivetti, Rafael Gomez-Bombarelli, Manuel Moliner,* and Yuriy Román-Leshkov*

Cite This: https://doi.org/10.1021/acsami.3c15810

Read Online

ACCESS | Metrics & More | Article Recommendations | Supporting Information

ABSTRACT: We report the one-pot synthesis of a chabazite (CHA)/erionite (ERI)-type zeolite intergrowth structure characterized by adjustable extents of intergrowth enrichment and Si/Al molar ratios. This method utilizes readily synthesizable 6-azaspiro[5.6]dodecan-6-ium as the exclusive organic structure-directing agent (OSDA) within a potassium-dominant environment. High-throughput simulations were used to accurately determine the templating energy and molecular shape, facilitating the selection of an optimally biselective OSDA from among thousands of prospective candidates. The coexistence of the crystal phases, forming a distinct structure comprising disk-like CHA regions bridged by ERI-rich pillars, was corroborated via rigorous powder X-ray diffraction and integrated differential-phase contrast scanning transmission electron microscopy (iDPC S/TEM) analyses. iDPC S/TEM imaging further revealed the presence of single offretite layers dispersed within the ERI phase. The ratio of crystal phases between CHA and ERI in this type of intergrowth could be varied systematically by changing both the OSDA/Si and K/Si ratios. Two intergrown zeolite samples with different Si/Al molar ratios were tested for the selective catalytic reduction (SCR) of NO_x with NH_3, showing competitive catalytic performance and hydrothermal stability compared to that of the industry-standard commercial NH_3-SCR catalyst, Cu-SSZ-13, prevalent in automotive applications. Collectively, this work underscores the potential of our approach for the synthesis and optimization of adjustable intergrown zeolite structures, offering competitive alternatives for key industrial processes.

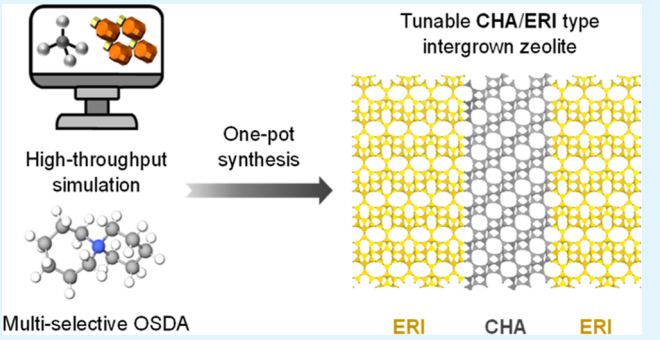

KEYWORDS: *small-pore zeolites, zeolite intergrowth, erionite (ERI), chabazite (CHA), selective catalytic reduction (SCR) of NO_x*

INTRODUCTION

Zeolites, with their unique porosity, diffusional pathways, and adjustable acid sites, have been extensively employed in industrial applications.[1,2] A distinct category within the zeolite family is zeolite intergrowths, which are formed through the coexistence of multiple crystal phases in a single crystal arising from particular lattice anomalies such as rotations, reflections, or translations.[3] This phase coexistence enables unique catalytic and diffusional properties to emerge depending on the local crystallographic environment within a pore. For example, prior studies have shown how stacking faults can modify product selectivity as well as permeation and selectivity properties.[4−6] Moreover, intergrown zeolites have demonstrated superior performance in the selective catalytic reduction (SCR) of NO_x compared to that of their pure-phase counterparts.[7−10]

However, the synthesis of intergrown zeolites is a challenging task, mainly due to the difficulties in controlling stacking disorders during crystallization. Among the existing approaches, one common strategy is to use two or more organic structure-directing agents (OSDAs) to control the intergrowth.[10−12] For example, mixing tetrapropylammonium (known to crystallize MFI)[13] with tetrabutylammonium (known to crystallize MEL)[14] generates intergrown ZSM-5/ZSM-11 zeolites,[12] which are akin to how mixtures of 15-crown-5 ether and 18-crown-6 ether are used to crystallize FAU/EMT intergrowths.[11] Similarly, Cu-tetraethylenepentamine, tetraethylammonium, and hexamethonium were used to crystallize the intergrowth of chabazite (CHA)/erionite (ERI).[10] However, the need for two or more OSDAs to crystallize zeolite intergrowth stresses the complexity and cost

Received: October 23, 2023
Revised: January 16, 2024
Accepted: January 22, 2024

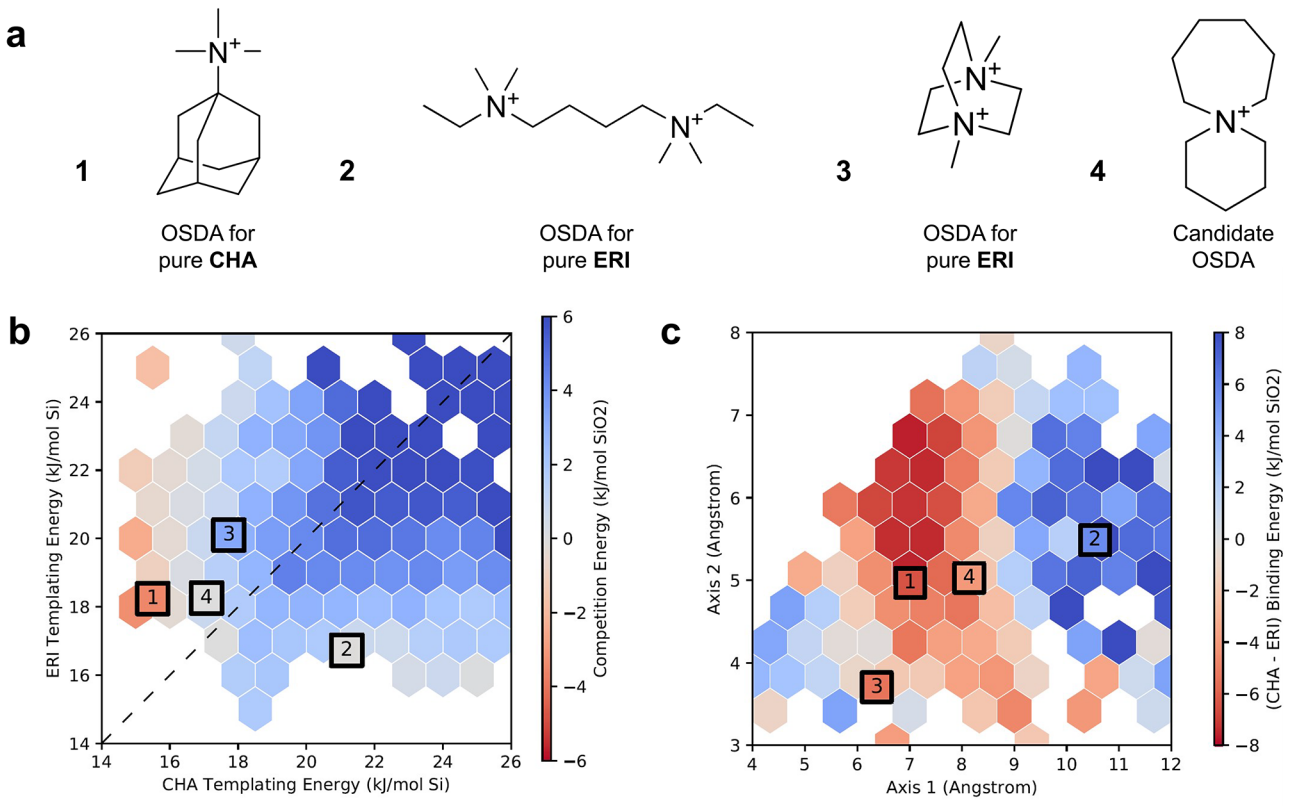

Figure 1. (a) OSDA reported to crystallize CHA and ERI with the candidate OSDA presented. (b) Comparison between the templating energies of the OSDAs with the CHA and ERI frameworks. (c) Relationship between the shape of the OSDAs and their binding energies toward CHA or ERI. Red (blue) indicates the more favorable binding energy toward CHA (ERI). Squares represent the energies/shapes of OSDAs shown in (a).

associated with such methods, requiring more streamlined and cost-effective approaches.[15]

Considering these limitations, we investigated the one-pot synthesis of a CHA/ERI intergrowth zeolite using a single multiselective OSDA. Our strategy relied on high-throughput screening simulations to determine the binding energies between thousands of organic molecules and hundreds of zeolite frameworks.[16−19] This methodology allowed us to identify those OSDA candidates with ideal shapes and binding energies for the simultaneous formation of the desired zeolite phases within the intergrowth.

Gratifyingly, we were able to synthesize a zeolite intergrowth comprising mainly CHA/ERI topologies with a minor component of single offretite (OFF) layers dispersed within the ERI phase. We employed a single OSDA, 6-azaspiro[5.6]-dodecan-6-ium hydroxide, identified by our high-throughput simulations. Further, the synthesis was carried out in a potassium-rich environment, and the resulting architecture was confirmed by integrated differential-phase contrast scanning transmission electron microscopy (iDPC S/TEM) and powder X-ray diffraction (PXRD). The ERI/OFF regions were highly enriched in ERI, with single OFF layers present as stacking faults. When ion-exchanged with Cu^{2+}, the zeolite intergrowths showed deNO_x activity and hydrothermal stability rivaling those of pure Cu-CHA materials with analogous physicochemical properties.

RESULTS AND DISCUSSION

We identified OSDAs having the necessary geometries and binding energies to facilitate the crystallization of the target zeolite phases in the intergrowth. Specifically, we applied our high-throughput simulation pipeline to compute the templating energies of each OSDA-zeolite pair, quantifying the directing potential of each OSDA. Templating energy—a weighted average of four distinct zeolite-OSDA binding energies defined in our prior work—serves as a quantitative metric of the likelihood of crystallizing the target zeolite framework with the specified OSDA.[18] N,N,N-Trimethyl-1-adamantylammonium (OSDA 1, Figure 1a) is known for templating the formation of CHA (SSZ-13), while both N^1,N^4-diethyl-N^1,N^1,N^4,N^4-tetramethylbutane-1,4-diaminium (OSDA 2, Figure 1a) and 1,4-dimethyl-1,4-diazabicyclo[2.2.2]octane-1,4-diium (OSDA 3, Figure 1a) govern the crystallization of ERI (UZM-12 and SSZ-98, respectively).[20,21] Figure 1b depicts the templating energy for CHA and ERI zeolite frameworks for OSDAs 1 through 4 against a density plot of previously calculated molecules. Here, OSDA 1 is situated on the left of the graph, indicating a high affinity for CHA, while OSDA 2 resides close to the bottom, signaling an affinity for ERI. OSDA 3, on the contrary, exhibits templating energy that strays from the preferred regions for ERI zeolite framework formation, leading to a constrained synthesis space for ERI and the emergence of competitive phases such as KFI and PST-29.[22,23] In the case of OSDA-3, it is evident that inorganic cations play an important role in directing phase competition to a specific topology.[24]

Figure 1c displays the measured dimensions of the two major axes for nearly 1,000 known OSDAs. Here, OSDAs 1 and 2 occupy distinct regions since both molecules have similar widths (ca. 5 Å) but different lengths (i.e., 7 Å vs 11 Å). We

https://doi.org/10.1021/acsami.3c15810
ACS Appl. Mater. Interfaces XXXX, XXX, XXX−XXX

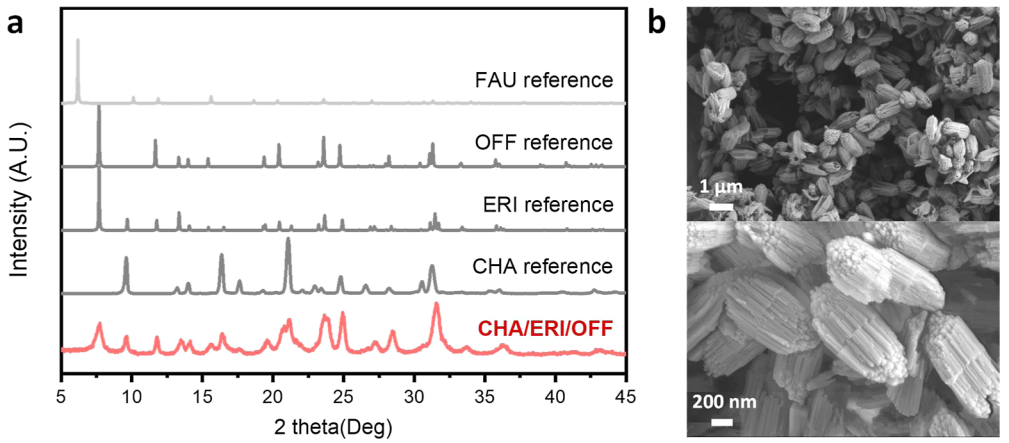

Figure 2. (a) PXRD patterns of the reference FAU, OFF, ERI, CHA, and calcined CHA/ERI/OFF sample. (b) SEM image of the calcined sample.

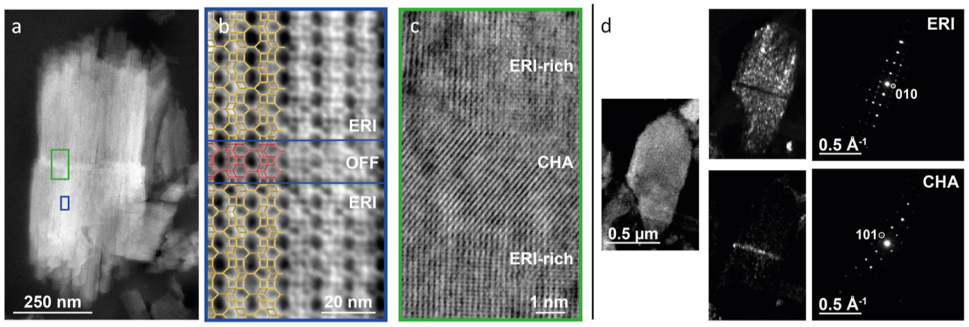

Figure 3. (a) ADF-S/TEM image of the CHA/ERI/OFF intergrown zeolite sample sectioned by using ultramicrotomy to a thickness of 50 nm. There is a CHA disc in the middle with ERI-rich epitaxial layers on both ends. (b) iDPC-S/TEM image of the ERI-rich region of the sample, marked in blue. The image reveals the AABAAC packing (ERI structure) with a layer of AAB packing (OFF structure), as depicted in Figure S5. (c) iDPC-S/TEM image of the CHA core region, marked in green in (a); the light area is identified as CHA and the gray area is a mixture of pure ERI and disordered ERI. (d) SED data shows characteristic CHA diffraction from the core disk close to the $[100]_{CHA}$ direction and characteristic ERI diffraction from both sides viewed along ~ $[100]_{ERI}$. Virtual dark-field maps based on the 010_{ERI}- and 101_{CHA}-reflections, respectively, show that the CHA is localized to the core disc with the ERI-rich material on the sides.

surmised that a singular OSDA molecule with the capacity to stabilize both the ERI and CHA phases in the intergrowth should exhibit intermediate characteristics to those of OSDAs 1 and 2, both in terms of energy and geometry. That is, the optimal OSDA should exhibit relatively low templating energies toward the two distinct frameworks constituting the desired intergrowth and also maintain a shape that not only stabilizes both frameworks but also promotes crystallization.[8] By applying these criteria to filter potential OSDAs, we identified 6-azaspiro[5.6]dodecan-6-ium (OSDA 4) as a promising candidate for synthesizing CHA/ERI intergrowths. This molecule exhibits templating energies favorable to both the CHA and ERI frameworks (as depicted in Figure 1b). Its templating energy resides near the coordinate origin and aligns almost symmetrically along the y = *x* axis toward both the CHA and ERI frameworks, indicating a potential to crystallize the CHA/ERI intergrowth. Additionally, as illustrated by the color-coded representation in Figure 1b, the minimal difference in competitive energies between CHA and ERI suggests that OSDA 4 demonstrates nearly equivalent structural directivity toward both CHA and ERI. Moreover, the geometric profile of OSDA 4 falls between those of OSDA 1 and 2, suggesting its suitability to simultaneously stabilize both *cha* and *eri* cages (refer to Figure 1c).

Next, we carried out a synthesis campaign to crystallize CHA/ERI intergrowths using OSDA 4. OSDA 4, synthesized in a one-step reaction, such as the delineation shown in Figure S1, was characterized utilizing both ^{1}H and ^{13}C nuclear magnetic resonance (NMR) spectroscopy (Figure S2). Earlier work by our research group established that OSDA 4 can facilitate the formation of the CHA framework in a sodium-rich environment.[18] In the present work, however, we used potassium to provide cations adept at stabilizing secondary building units present in both CHA and ERI. Synthesis gels with compositions of 1 SiO_2: 0.03−0.17 Al: 0.2−0.4 OSDA: 0.1−0.3 KOH: 15 H_2O were subjected to hydrothermal conditions at 140−175 °C for 7 days. PXRD analysis of the crystalline product predominantly revealed the coexistence of CHA and ERI phases, albeit minor beta phase impurities were detected in certain gel compositions (indicated by an asterisk in Figure S3).

To mitigate the crystallization of the undesired beta zeolite phase, two distinct strategies were deployed. One approach involved the introduction of H-CHA seeds into the synthesis gels (Figure S3). It is worth noting that the intensity of the characteristic CHA diffraction peak at 9.5° was found to be independent of the quantity of the CHA seed added, corroborating that the CHA phase in the samples is not sourced from the seed. Another approach was to use sodium as a costructure-directing agent to further drive the crystallization process toward the CHA phase. Figure S4 depicts the PXRD patterns of samples synthesized in a mixed sodium and

https://doi.org/10.1021/acsami.3c15810
ACS Appl. Mater. Interfaces XXXX, XXX, XXX−XXX

Table 1. Synthesis Table from Different FAU Sources: (a) CBV-712 (Zeolyst, Si/Al = 6), (b) CBV-720 (Zeolyst, Si/Al = 15), and (c) CBV-760 (Zeolyst, Si/Al = 30)[a]

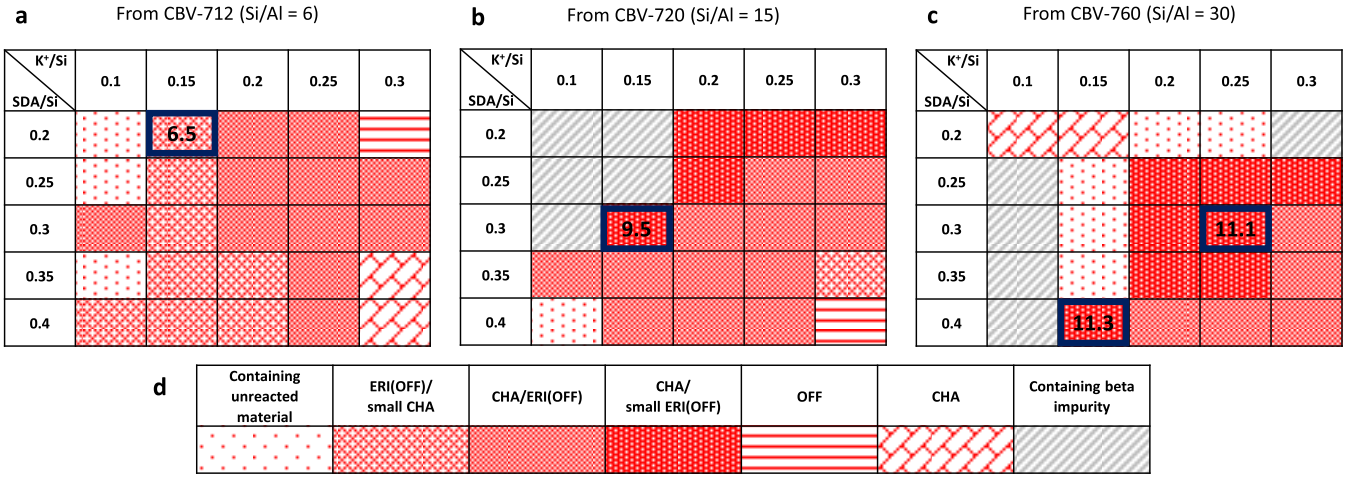

[a]The H_2O/Si ratio was fixed to 15, and the crystallization was performed at 160 °C for 7 days. The color code at (d) shows the results of each crystallization characterized with PXRD. Unreacted material includes amorphous and FAU precursors. The values marked in the bold box indicate the highest Si/Al ratios of the CHA/ERI(OFF)-type materials confirmed with ICP-AES.

potassium environment without the use of the CHA seed. A significant beta impurity peak (* in Figure S4) was discernible in samples with small quantities or the absence of sodium (Na/K ≤ 0.05). However, with an optimal balance of sodium and potassium (0.1 ≤ Na/K ratio ≤3), the diffraction pattern shows the exclusive presence of both CHA and ERI phases. When exceeding this ratio (i.e., Na/K ≥ 4), only the CHA framework was observed. Using this information, we selected an optimal gel composition: 1 SiO_2: 0.17 Al: 0.3 OSDA: 0.2 KOH: 15 H_2O. This was subjected to a temperature of 160 °C over a period of 7 days, followed by calcination in an air environment at 580 °C for 6 h. The resulting crystals gave rise to the red PXRD pattern depicted in Figure 2a. This pattern features peaks at 7.8 and 9.5° 2θ angles, which correspond to the ERI/OFF and CHA frameworks, respectively.

Quantifying the phase enrichment between these phases using PXRD is challenging and requires the use of additional techniques. The SEM image in Figure 2b reveals a uniform crystal structure featuring rod-like crystals emerging from a thin central layer. The consistent morphology negates the potential for a physical mixture of crystals with distinct topologies. The crystal structure of the zeolite sample was further investigated via iDPC-S/TEM imaging and scanning electron diffraction (SED). The cross-sectional image of the crystal shown in Figure 3a reveals a thin central disk that is framed by rod-like epitaxial layers on both sides. Detailed inspection of the central disc (as indicated by the blue box in Figures 3a and S6) revealed a CHA domain with a thickness of approximately 20 nm. In contrast, the protruding structures surrounding the central disc (demarcated by the green box in Figure 3a) comprised predominantly ERI-rich domains intermittently interspersed with single OFF layers (Figures 3b,c and S5). The ERI and OFF structures are assembled from *can* cages that adhere to ABAB and AAAA sequences, respectively. Virtual dark field mapping of the SED data validates this configuration (Figures 3d and S7).

Energy-dispersive X-ray (EDX) spectroscopy analysis revealed Si/Al ratios of 9.0 for the CHA core and 6.3 for the ERI-rich domains (Figure S8). The discrepancy in the atomic topology between the CHA core and ERI-rich shells implies a potential shift in the overall Si/Al ratio of the material. This is noteworthy as the Si/Al ratio may have direct implications for the performance and stability of the catalyst, contingent upon the relative ratios of the CHA cores and ERI-rich shells. Consequently, a CHA-enriched intergrown catalyst might exhibit higher overall Si/Al ratios as compared to those of an ERI-enriched intergrowth. To the best of our knowledge, this is the first triphasic intergrown zeolite synthesized using a single OSDA.

The morphology of zeolite intergrowth is significantly influenced by the crystal size. Specifically, when the crystal size is below 200 nm, the derived intergrown material shows a unique morphology that deviates from the morphology of larger crystals. These smaller crystals show an intergrowth reminiscent of domains, where CHA domain "islands" appear dispersed within ERI-rich regions. This stands in contrast to the morphology of larger crystals, which present CHA-domains centrally and ERI-domains extending from both ends. The PXRD pattern of this domain-like intergrown sample, as depicted in Figure S9a, presents a characteristic CHA/ERI-type intergrown material pattern. However, due to the smaller crystal size, each representative peak appears somewhat broader. The SEM image (Figure S9b) shows a particle size less than 200 nm, while the virtual dark field mapping of the SED data, along with the iDPC-S/TEM (Figure S9c,d), further supports the idea of dispersed CHA islands throughout the ERI region. This domain-like intergrowth represents a potential catalyst for the NH_3-SCR reaction; however, achieving the perfect random alternation of CHA and ERI domains poses a considerable challenge. Therefore, generating an alternating type of CHA/ERI intergrown zeolite will be reserved for future studies.

Although the precise mechanism and crystal growth kinetics of the intergrowth are currently being investigated, the formation of a triphasic crystal can be rationalized by crystallization heuristics and density functional theory (DFT) calculations. First, the CHA/ERI-type intergrowth features structural motifs in the form of cancrinite (*can*), *cha*, and *swy* cavities, as illustrated in Figure S10a. Prior reports have shown that potassium cations provide stability to the formation of *can*

https://doi.org/10.1021/acsami.3c15810
ACS Appl. Mater. Interfaces XXXX, XXX, XXX−XXX

Table 2. Synthesis Conditions and Properties of Cu-CHA/ERI (4.4) and Cu-CHA/ERI (6.7), Which Were Synthesized with the Gel Compositions of 1 SiO_2: 0.17 Al: 0.3 SDA: 0.2 KOH: 15 H_2O, 5 wt % CHA Seed Using CBV-712 as a Starting Precursor and 1 SiO_2: 0.07 Al: 0.3 SDA: 0.2 KOH: 15 H_2O, 5 wt % H-SSZ-13 Seed Using CBV-720 as a Starting Material for 7 Days at 175 °C, Respectively[a]

sample	product	textural properties			ICP after ion-exchange			aging condition
	crystal size [μm]	surface area [m^2/g]	micropore volume [cc/g]	micropore area [m^2/g]	Si/Al	% K	% Cu	
Cu-CHA/ERI (4.4)	1−1.2	480	0.135	313	4.4	4.5	3.5	600 °C 16 h
Cu-CHA/ERI (6.7)	0.8−1	605	0.196	460	6.7	1.5	3.6	750 °C 13 h

[a]Both catalysts were characterized with PXRD and iDPC S-TEM to confirm the CHA/ERI-type intergrown materials.

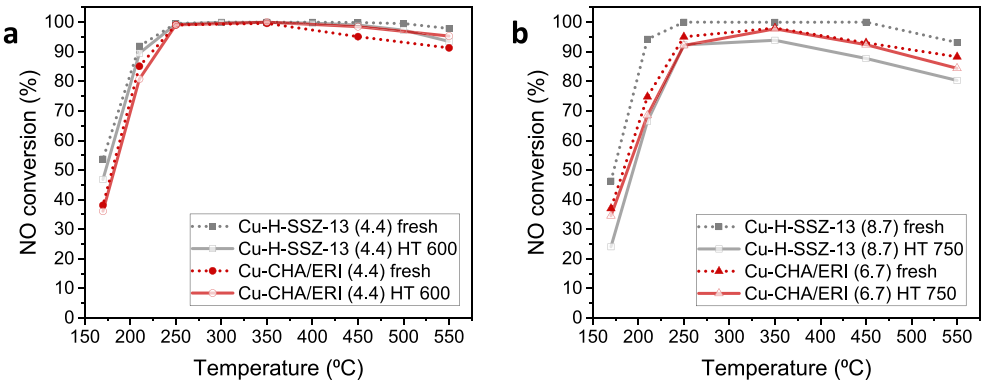

Figure 4. Catalytic results for NH_3-SCR of NO_x. NO conversion results from fresh calcined catalyst (dashed line) and aged catalyst (solid line) of (a) low-Si SSZ-13 (4.4) and CHA/ERI (4.4) and (b) intermediate-Si SSZ-13 (8.7) and CHA/ERI (6.7). The value in parentheses indicates the Si/Al ratio confirmed with ICP-AES after ion-exchange.

cages, which are crucial components of building ERI layers. Second, in our previous work, we documented that OSDA 4 stabilizes the *cha* cavity, which is essential for the formation of the CHA framework.[18] Indeed, the most favorable binding energy is exhibited by the optimal crystallographic conformer of OSDA 4, as shown in Figure S10b. Finally, the interface of single OFF layers with the ERI domains forms a unique *swy* cavity, where DFT calculations indicate that two OSDAs can colocate within a *swy* cavity to stabilize the organic−inorganic complex (see Figure S10c). This calculation is coherent with our thermogravimetric results, which reveal that 2−3 OSDAs are occluded within the 36 tetrahedral sites of the framework (details in the Supporting Information). Therefore, these findings imply that the large cavities in the CHA/ERI-type intergrowth are predominantly occupied by the OSDA, which is in line with our calculations that affirm the significant role of the OSDA in stabilizing these cavities.

Considering the novel nature of the CHA/ERI-type intergrown material, we undertook synthesis campaigns, modifying the synthetic parameters within the precursor gels, to understand the key aspects of this intergrowth, including its synthesis window, tunability of phase enrichment, and range of accessible Si/Al ratios. We found that the enrichment of the CHA and ERI in the intergrown material can be controlled by adjusting the relative amounts of potassium and OSDA. A qualitative determination of each phase's relative abundance can be made based on the characteristic peak areas' ratios at 7.8 and 9.5° 2θ regions. Specifically, at the gel composition of 1 SiO_2: 0.17 Al: 0.35 OSDA: 0.1−0.3 KOH: 15 H_2O, with 5 wt % of the CHA seed, different portions of CHA/ERI/OFF phases surfaced after 7 days at 160 °C. When the K/Si ratio is 0.15, the resultant zeolite leans toward an ERI(OFF)-rich character. Increasing potassium content to 0.3, with other ratios held constant (green arrow in Figure S11), resulted in decreasing relative peak areas at the 7.8 to 9.5° 2θ region, suggesting a shift toward CHA character.

Table 1 provides synthesis conditions for crystallizing the CHA/ERI-type intergrowth zeolites from a variety of FAU precursors used as Si and Al sources. Holding the H_2O/Si ratio constant at 15, we successfully produced the intergrown zeolites using different concentrations of OSDA and potassium relative to Si, as demonstrated in the PXRD patterns in Figures S12−14. When the synthesis gel's OH/Si ratio was very low or high, beta and CHA were observed. Using FAU zeolites as the silicon source facilitated the creation of CHA/ERI-type intergrown zeolites across a wide synthesis window. Interestingly, using a FAU with a higher Si/Al ratio shifted the synthesis window toward a region requiring higher pH and cation concentrations for crystallization.

The variation in the relative peak intensities at 9.5° 2θ (CHA) and 7.8° 2θ (ERI) regions provides a key to understanding the synthesis space. The categorization of intergrowths in Table 1d, determined by a relative peak intensity cutoff of 1.5, uncovers preferential conditions for each phase's enrichment, which, in essence, implies a systematic control of CHA or ERI(OFF) proportions within the CHA/ERI-type intergrowth by adjusting OSDA/Si and K/Si ratios. This ability to regulate phase enrichment can be instrumental in fine-tuning the catalyst design for specific applications.

The values inside the bold box in Table 1 indicate the highest Si/Al ratios of the intergrown materials after 7 days of crystallization at 160 °C, as confirmed with inductively coupled plasma atomic emission spectroscopy (ICP-AES). Using FAU precursors with a high Si/Al ratio showed a concomitantly higher Si/Al ratio in the product zeolites. The trend implied that there was a loss of silicon atoms from the precursors that

https://doi.org/10.1021/acsami.3c15810
ACS Appl. Mater. Interfaces XXXX, XXX, XXX−XXX

were not used for the crystallization of the intergrowth. The loss of silicon atoms in the final product aligns with the EDX results in Figure S8, where the low-Si ERI domains decrease the overall Si/Al ratio of the intergrowth. However, the Si/Al ratio >11 appears to be the highest among all the reported CHA/ERI-type materials. As shown in Figure S11, the Si/Al ratio in the same type of intergrowth tends to decrease toward the lower right of the synthesis table, which represents higher OH/Si molar ratios, since there are more organic and inorganic structure-directing cations to incorporate aluminum atoms inside the intergrowth. Hence, the values inside the bold boxes, located in the upper left corner of the synthesis table, are expected to be the highest Si/Al ratios achievable in this system.

Future demand for SCR catalysts in heavy-duty vehicles will likely call for zeolite-based catalysts with midrange Si/Al ratios between 4.5 and 7.[25] Accordingly, we prepared two samples within these ranges (see Table 2 for synthesis conditions and chemical compositions and Figures S15 and S16 for thermogravimetric analysis and solid-state NMR characterization) and ion-exchanged them with 3.5 wt % of Cu for evaluation as catalysts in the NH_3-SCR of NO_x.

The Cu-exchanged zeolites were tested under conditions resembling those encountered in heavy-duty applications by employing a feed composition of 500 ppm of NO, 500 ppm of NH_3, 5% of steam, and 7% of oxygen with a gas hourly space velocity (GHSV) as high as 450,000 mL/($h.g_{cat}$) at a wide range of reaction temperatures (170−550 °C).[8,26,27] The catalysts showed remarkable NO_x conversion, as shown in Figure 4. The NO conversion values were comparable to those of the Cu−CHAs with similar Si/Al ratios.[8,26] Notably, the CHA/ERI-type intergrown zeolite samples showed stable catalytic profiles when subjected to high-temperature steam treatments at 600 and 750 °C, which are well-established aging treatments to evaluate catalyst stability for heavy-duty diesel vehicles.[25] The sustained activity of these Al-rich zeolites, even after hydrothermal treatment at 600 and 750 °C, suggests their structural stability, likely attributed to the selection of an optimal OSDA. This structural stability is further evidenced by the PXRD patterns presented in Figure S17. While some of the characteristic peaks have diminished after a harsh hydrothermal treatment, the catalysts' crystallinity still remains notably high. While the low-Si Cu-CHA/ERI (4.4) showed analogous stability compared to that of its CHA counterpart, the medium-Si Cu-CHA/ERI (6.7) showed a slight improvement of its stability after being aged compared to that of its CHA counterpart (Figure 4), while producing an insignificant amount of N_2O byproduct, as shown in Figure S18. The excellent hydrothermal stability and high deNO_x conversion suggest that the CHA/ERI-type intergrown zeolites can be applicable to NH_3-SCR under conditions relevant to heavy-duty diesel applications.[25]

CONCLUSIONS

In this study, we have successfully synthesized a unique CHA/ERI-type intergrown zeolite using a single OSDA, meticulously selected through high-throughput simulations. This approach resulted in a distinctive triple intergrowth structure composed of a central CHA disc core encapsulated by ERI-rich domains. Notably, the proportion of each phase in the intergrowth can be effectively modulated by adjusting the OSDA concentration or the ratio of cations within the precursor gels. This allows the Si/Al ratios within the intergrowth to vary from low (4) to moderate (11), demonstrating the versatility of our methodology. Furthermore, the intergrown zeolite samples exhibit excellent catalytic performance in the NH_3-SCR reaction and excellent hydrothermal stability, making them a potential candidate for rigorous applications such as heavy-duty diesel engines. We believe that the strategic deployment of high-throughput simulations to identify the feasible and optimal OSDA and the methodology used to synthesize the CHA/ERI-type intergrowth set a robust foundation for controlling the phases of other complex zeolite intergrowth structures, thereby unlocking further potential in the field of zeolite synthesis and catalysis.

ASSOCIATED CONTENT

Supporting Information

The Supporting Information is available free of charge at https://pubs.acs.org/doi/10.1021/acsami.3c15810.

All experimental methods; catalyst characterization; synthesis scheme of Aza-56 OSDA; ^1H and ^{13}C NMR spectra; influence of the H-CHA seed concentration on the crystallization of CHA/ERI-type intergrowth materials; PXRD patterns; iDPC S/TEM images; virtual dark field images; elemental mapping and EDX spectroscopy analysis; characterization of the CHA/ERI-type intergrowth sample 3; important cages and cavities in the CHA/ERI/OFF intergrowth, OSDA 4 stabilizing *cha* cavity, and *swy* cavity stabilized by two molecules of OSDA 4; tunable enrichment and final Si/Al ratios; thermogravimetric analysis; ^{29}Si and ^{27}Al solid-state NMR results; and N_2O yield (ppm) of low-Si Cu-CHA/ERI (4.4) and intermediate-Si Cu-CHA/ERI (6.7) (PDF)

AUTHOR INFORMATION

Corresponding Authors

Yuriy Román-Leshkov − *Department of Chemical Engineering, Massachusetts Institute of Technology, Cambridge, Massachusetts 02139, United States;* orcid.org/0000-0002-0025-4233; Email: yroman@mit.edu

Manuel Moliner − *Instituto de Tecnología Química, Universitat Politècnica de València-Consejo Superior de Investigaciones Científicas, 46022 Valencia, Spain;* orcid.org/0000-0002-5440-716X; Email: mmoliner@itq.upv.es

Authors

Soonhyoung Kwon − *Department of Chemical Engineering, Massachusetts Institute of Technology, Cambridge, Massachusetts 02139, United States*

Estefanía Bello-Jurado − *Instituto de Tecnología Química, Universitat Politècnica de València-Consejo Superior de Investigaciones Científicas, 46022 Valencia, Spain*

Evgeniia Ikonnikova − *Department of Materials and Environmental Chemistry, Stockholm University, SE-106 91 Stockholm, Sweden*

Hwajun Lee − *Department of Chemical Engineering, Massachusetts Institute of Technology, Cambridge, Massachusetts 02139, United States*

Daniel Schwalbe-Koda − *Department of Material Science and Engineering, Massachusetts Institute of Technology, Cambridge, Massachusetts 02139, United States*

Avelino Corma − *Instituto de Tecnología Química, Universitat Politècnica de València-Consejo Superior de Investigaciones Científicas, 46022 Valencia, Spain;* orcid.org/0000-0002-2232-3527

Tom Willhammar − *Department of Materials and Environmental Chemistry, Stockholm University, SE-106 91 Stockholm, Sweden;* orcid.org/0000-0001-6120-1218

Elsa A. Olivetti − *Department of Material Science and Engineering, Massachusetts Institute of Technology, Cambridge, Massachusetts 02139, United States;* orcid.org/0000-0002-8043-2385

Rafael Gomez-Bombarelli − *Department of Material Science and Engineering, Massachusetts Institute of Technology, Cambridge, Massachusetts 02139, United States;* orcid.org/0000-0002-9495-8599

Complete contact information is available at: https://pubs.acs.org/10.1021/acsami.3c15810

Author Contributions

All authors have given approval to the final version of the manuscript.

Funding

S.K. acknowledges partial funding from Designing Materials to Revolutionize and Engineer our Future (DMREF) from the National Science Foundation (NSF) 1922311, 1922372, and 1922090 awards. S.K. was additionally funded by the Kwanjeong Educational Fellowship. T.W. and E.I. acknowledge financial support from the Swedish Research Council (grant no. 2019-05465) and the Swedish Research Council for Sustainable Development, FORMAS (grant no. 2022-01270). E.B., A.C., and M.M. acknowledge funding from the Spanish Government through PID2021-122755OB-I00 funded by MCIN/AEI/10.13039/501100011033 and TED2021-130739B-I00 funded by MCIN/AEI/10.13039/501100011033/EU/PRTR, and from Generalitat Valenciana through AICO/2021/201. The authors are also thankful for the Severo Ochoa financial support from the Spanish Ministry of Science and Innovation (CEX2021-001230-S/funding by MCIN/AEI/10.13039/501100011033). E.B. acknowledges the Spanish Government for an FPI scholarship (PRE2019-088360).

Notes

The authors declare no competing financial interest.

■ ACKNOWLEDGMENTS

This work made use of the MRSEC and DCIF Shared Experimental Facilities at MIT.

■ ABBREVIATIONS

CHA, chabazite
ERI, erionite
OFF, offretite
OSDA, organic structure-directing agent
PXRD, powder X-ray diffraction
iDPC S/TEM, integrated differential-phase contrast scanning transmission electron microscopy
NMR, nuclear magnetic resonance
ICP-AES, inductively coupled plasma atomic emission spectroscopy
SCR, selective catalytic reduction
GHSV, gas hourly space velocity

■ REFERENCES

(1) Li, Y.; Li, L.; Yu, J. Applications of Zeolites in Sustainable Chemistry. *Chem* **2017**, *3* (6), 928−949.
(2) Martínez, C.; Corma, A. Inorganic Molecular Sieves: Preparation, Modification and Industrial Application in Catalytic Processes. *Coord. Chem. Rev.* **2011**, *255* (13−14), 1558−1580.
(3) Willhammar, T.; Zou, X. Stacking Disorders in Zeolites and Open-frameworks - Structure Elucidation and Analysis by Electron Crystallography and X-ray Diffraction. *Z. Kristallogr. - Cryst. Mater.* **2013**, *228* (1), 11−27.
(4) Chen, N. Y.; Schlenker, J. L.; Garwood, W. E.; Kokotailo, G. T. TMA-offretite. Relationship Between Structural and Catalytic Properties. *J. Catal.* **1984**, *86* (1), 24−31.
(5) Kumar, P.; Kim, D. W.; Rangnekar, N.; Xu, H.; Fetisov, E. O.; Ghosh, S.; Zhang, H.; Xiao, Q.; Shete, M.; Siepmann, J. I.; Dumitrica, T.; McCool, B.; Tsapatsis, M.; Mkhoyan, K. A. One-dimensional Intergrowths in Two-dimensional Zeolite Nanosheets and Their Effect on Ultra-selective Transport. *Nat. Mater.* **2020**, *19* (4), 443−449.
(6) Millward, G. R.; Ramdas, S.; Thomas, J. M. On the Direct Imaging of Offretite, Cancrinite, Chabazite and other Related ABC-6 Zeolites and their Intergrowths. *Proc. R. Soc. London, Ser. A* **1985**, *399* (1816), 57−71.
(7) Arulraj, K.; Chandler, G. R.; Collier, J.; Garcia, R.; Green, A.; McNamara, N.; Phillips, P.; Ruggeri, M. P.; Turrina, A. Jmz-12, a Disordered aei/cha Family of Zeolites, its Synthesis and Use. EP4098616, 2022.
(8) Bello-Jurado, E.; Schwalbe-Koda, D.; Nero, M.; Paris, C.; Uusimäki, T.; Román-Leshkov, Y.; Corma, A.; Willhammar, T.; Gómez-Bombarelli, R.; Moliner, M. Tunable CHA/AEI Zeolite Intergrowths with A Priori Biselective Organic Structure-Directing Agents: Controlling Enrichment and Implications for Selective Catalytic Reduction of NOx. *Angew. Chem., Int. Ed.* **2022**, *61* (28), No. e202201837.
(9) Naraki, Y.; Ariga, K.; Nakamura, K.; Okushita, K.; Sano, T. ZTS-1 and ZTS-2: Novel Intergrowth Zeolites with AFX/CHA Structure. *Microporous Mesoporous Mater.* **2017**, *254*, 160−169.
(10) Sree, S. P.; Verheyen, E.; De Prins, M.; Van Der Donck, T.; Van Tendeloo, L.; Schuetze, F.; Martens, J. A. Synthesis of a New Zeolite, Intergrowth of Erionite and Chabazite. *ACS Mater. Lett.* **2021**, *3* (5), 658−662.
(11) John, N. S.; Stevens, S. M.; Terasaki, O.; Anderson, M. W. Evolution of Surface Morphology with Introduction of Stacking Faults in Zeolites. *Chem. Eur. J.* **2010**, *16* (7), 2220−2230.
(12) Millward, G. R.; Ramdas, S.; Thomas, J. M.; Barlow, M. T. Evidence for Semi-regularly Ordered Sequences of Mirror and Inversion Symmetry Planes in ZSM-5/ZSM-11 Shape-selective Zeolitic Catalysts. *J. Chem. Soc., Faraday Trans. 2* **1983**, *79*, 1075−1082.
(13) Robert J Argauer, G. R. L. Crystalline Zeolite zsm-5 and Method of Preparing the Same. US3702886A, 1969.
(14) Chu, P. Crystalline Zeolite zsm-11. US3709979A, 1970.
(15) Muraoka, K.; Chaikittisilp, W.; Okubo, T. Multi-objective De Novo Molecular Design of Organic Structure-Directing Agents for Zeolites Using Nature-Inspired Ant Colony Optimization. *Chem. Sci.* **2020**, *11* (31), 8214−8223.
(16) Schwalbe-Koda, D.; Gómez-Bombarelli, R. Benchmarking Binding Energy Calculations for Organic Structure-Directing Agents in Pure-Silica Zeolites. *J. Chem. Phys.* **2021**, *154* (17), 174109.
(17) Schwalbe-Koda, D.; Gómez-Bombarelli, R. Supramolecular Recognition in Crystalline Nanocavities through Monte Carlo and Voronoi Network Algorithms. *J. Phys. Chem. C* **2021**, *125* (5), 3009−3017.
(18) Schwalbe-Koda, D.; Kwon, S.; Paris, C.; Bello-Jurado, E.; Jensen, Z.; Olivetti, E.; Willhammar, T.; Corma, A.; Román-Leshkov, Y.; Moliner, M.; Gómez-Bombarelli, R. A Priori Control of Zeolite Phase Competition and Intergrowth with High-Throughput Simulations. *Science* **2021**, *374* (6565), 308−315.

(19) Schwalbe-Koda, D.; Santiago-Reyes, O. A.; Corma, A.; Román-Leshkov, Y.; Moliner, M.; Gómez-Bombarelli, R. Repurposing Templates for Zeolite Synthesis from Simulations and Data Mining. *Chem. Mater.* **2022**, *34* (12), 5366−5376.
(20) Lee, J. H.; Park, M. B.; Lee, J. K.; Min, H. K.; Song, M. K.; Hong, S. B. Synthesis and Characterization of ERI-type UZM-12 Zeolites and Their Methanol-to-olefin Performance. *J. Am. Chem. Soc.* **2010**, *132* (37), 12971−12982.
(21) Xie, D. Rational Design and Targeted Synthesis of Small-Pore Zeolites with the Assistance of Molecular Modeling, Structural Analysis, and Synthetic Chemistry. *Ind. Eng. Chem. Res.* **2021**, *60* (43), 15403−15415.
(22) Dusselier, M.; Davis, M. E. Small-Pore Zeolites: Synthesis and Catalysis. *Chem. Rev.* **2018**, *118*, 5265−5329.
(23) Lee, H.; Shin, J.; Choi, W.; Choi, H. J.; Yang, T.; Zou, X.; Hong, S. B. PST-29: A Missing Member of the RHO family of Embedded Isoreticular Zeolites. *Chem. Mater.* **2018**, *30* (19), 6619−6623.
(24) Shin, J.; Jo, D.; Hong, S. B. Rediscovery of the Importance of Inorganic Synthesis Parameters in the Search for New Zeolites. *Acc. Chem. Res.* **2019**, *52* (5), 1419−1427.
(25) Vennestrøm, P. N.; Thøgersen, J. R.; Gabrielsson, P. L. T.; Van Tendeloo, L.; Schütze, F. W.; Moliner, M. Advances and Perspectives From a Decade of Collaborative Efforts on Zeolites for Selective Catalytic Reduction of NOx. *Microporous Mesoporous Mater.* **2023**, *358*, 112336.
(26) Bello, E.; Ferri, P.; Nero, M.; Willhammar, T.; Millet, I.; Schütze, F. W.; van Tendeloo, L.; Vennestrøm, P. N.; Boronat, M.; Corma, A.; Moliner, M. NH_3-SCR Catalysts for Heavy-Duty Diesel Vehicles: Preparation of CHA-type Zeolites with Low-cost Templates. *Appl. Catal., B* **2022**, *303*, 120928.
(27) Zhu, J.; Liu, Z.; Xu, L.; Ohnishi, T.; Yanaba, Y.; Ogura, M.; Wakihara, T.; Okubo, T. Understanding the High Hydrothermal Stability and NH_3-SCR Activity of the Fast-synthesized ERI Zeolite. *J. Catal.* **2020**, *391*, 346−356.

https://doi.org/10.1021/acsami.3c15810
ACS Appl. Mater. Interfaces XXXX, XXX, XXX−XXX